Proceedings of the 2003 IEEE International Frequency Control Symposium and PDA Exhibition
Jointly with the 17th European Frequency and Time Forum

HIGH CONTRAST SIGNAL IN A COHERENT POPULATION TRAPPING BASED ATOMIC FREQUENCY STANDARD APPLICATION

M. Zhu
Agilent Laboratories, 3500 Deer Creek Road, Palo Alto, CA 94304, USA

Abstract – **A polarization-selective method [1] is developed for detecting a coherent-population-trapping (CPT) resonance signal in a vapor cell. The method uses a single laser beam with frequency modulation to induce CPT resonance and to control the AC Stark shift. The method provides a CPT resonance signal with a high contrast of 22%. Using this method, a CPT-based rubidium vapor cell frequency standard demonstrates a measured short-term stability of $1.4 \times 10^{-12}\ \tau^{-1/2}$.**

Keywords **- Coherent population trapping, AC Stark shift, polarization-selective detection**

I. INTRODUCTION

The coherent-population-trapping (CPT) based vapor cell frequency standard recently attracted a lot of interest for its potential to realize a compact, low cost frequency standard [2, 3, 4]. As in any optically-pumped frequency standard, the AC Stark shift (light shift) plays an important role in CPT-based frequency standards [4]. One of the methods to suppress the AC Stark shift is to use additional optical frequency components [4, 5, 6]. Especially, by choosing a proper modulation index, one can use the ±1st order sidebands of a frequency-modulated laser to induce CPT, and use the higher order sidebands of the same laser to suppress the AC Stark shift.

One prefers that the frequency components for AC Stark shift suppression are detuned from the atomic absorption profile so that they do not interfere with the CPT generation process severely. Thus they are not absorbed substantially when they traverse the atomic vapor cell. These frequency components form a constant background for the photo-detector, and limit the achievable signal contrast for CPT detection. Previously a CPT resonance signal with a contrast of 4.4% was reported [4]. The contrast in this case can be improved by increasing the laser intensity at the expense of broadened linewidth and increased AC Stark shift sensitivity.

In order to increase the CPT resonance signal contrast without further broadening the linewidth and without further increasing the AC Stark shift sensitivity, it is desirable to reduce the amount of optical power from the AC Stark shift controlling frequency components on the photo-detector. In the case where the AC Stark shift controlling frequency components can be separated from the CPT-generating frequency components spatially, the CPT-generating beam and the AC Stark shift controlling beam can be arranged to co-propagate with a small angle, or counter-propagate. The more complex optics setup required here makes it difficult to be used in compact frequency standards. In the case where the AC Stark shift controlling frequency components have a different polarization state from the one for the CPT-generating frequency components, the AC Stark shift controlling beam can be kept away from the photo-detector, at least partially. When only a single laser is used for this case, a modulator outside of the laser cavity (and possibly other optics) is needed to assign the two groups of frequency components with different polarization states.

On the other hand, the frequency components carrying the CPT resonance signal can be filtered out in the optical frequency domain, e.g., using an interferometer with a suitable free spectral range. This method has less limitation on the laser source. But the difficulty would be to maintain the stable resonance frequency for filtering and to keep the stable alignment of the optics involved.

Here we describe a polarization-selective method for CPT signal detection to achieve high signal contrast while keeping the AC Stark shift suppressed. This method utilizes a single laser beam for CPT-generation and AC Stark shift control so that it could be used in a compact vapor cell frequency standard.

II. THEORY

A. Atomic Dichroism and Atomic Birefringence in CPT

References [7] and [8] provide details of the theory of coherent population trapping. Here we only give a physical argument about the atomic dichroism and atomic birefringence in CPT as well as some numerical calculation results.

The interaction Hamiltonian in the Schrödinger representation can be written as

$$\hat{H}_I = \frac{1}{2}\hbar\Omega_{R1}e^{-i\omega_{L1}t}|e\rangle\langle g_1| + \text{h.c.} + \frac{1}{2}\hbar\Omega_{R2}e^{-i\omega_{L2}t}|e\rangle\langle g_2| + \text{h.c.} \quad (1)$$

where ω_{Lj} (j = 1, 2) is the angular frequency of the laser field that induces a transition from the ground state $|g_j\rangle$ (j = 1, 2) to the common excited state $|e\rangle$, the Rabi frequency Ω_{Rj} (j = 1, 2) describes the strength of the interaction between the laser field and the atom, and h.c. stands for Hermitian conjugate. The coherence between the two ground states results in a dark state

$$|\text{dark state}\rangle = \frac{\Omega_{R2}}{\Omega}e^{i\omega_{L1}t}|g_1\rangle - \frac{\Omega_{R1}}{\Omega}e^{i\omega_{L2}t}|g_2\rangle \quad (2)$$

where $\Omega = \sqrt{\Omega_{R1}^2 + \Omega_{R2}^2}$ is a normalization factor. Because the two interaction terms in (1) cancel each other, the dark state satisfies

$$\langle e|\hat{H}_I|\text{dark state}\rangle = 0 \tag{3}$$

In CPT-based frequency standards, often the hyperfine states $|F = I \pm 1/2, M_F = 0\rangle$ in the ground state of alkali atoms are chosen as $|g_1\rangle$ and $|g_2\rangle$. Due to the symmetry of the LS-coupling [9, 10], light with circular polarization (either σ^+ or σ^-) is used for CPT generation. It is expected that the atoms display both dichroism and birefringence when they are pumped with circular-polarized light [11]. It is also expected that both the atomic dichroism and the atomic birefringence change when the CPT resonance condition is approximately satisfied because of the atomic population trapped in the states $|g_1\rangle$ and $|g_2\rangle$. Using a separate probing laser beam, the atomic dichroism and atomic birefringence induced by a pumping laser beam are detected in Doppler-free laser spectroscopy [12] as well as in CPT [2].

As an example, Fig. 1 shows part of the energy levels for the ^{87}Rb atom. We assume that the Rabi frequencies for the transitions $|F=1\rangle \leftrightarrow |F'=2\rangle$ and $|F=2\rangle \leftrightarrow |F'=2\rangle$ are the same to keep the discussion simple. Due to the properties of the LS-coupling [9, 10], the Rabi frequencies for the transitions $|F=1\rangle \leftrightarrow |F'=1\rangle$ and $|F=2\rangle \leftrightarrow |F'=1\rangle$ are also the same. Both the σ^+-polarization and the σ^--polarization are derived from a single laser beam with linear polarization by aligning a quarter waveplate properly. Most of the optical power is in the σ^+-polarization for generating CPT. The optical power in the σ^--polarization is very weak so that it does not interfere with the CPT generation process substantially.

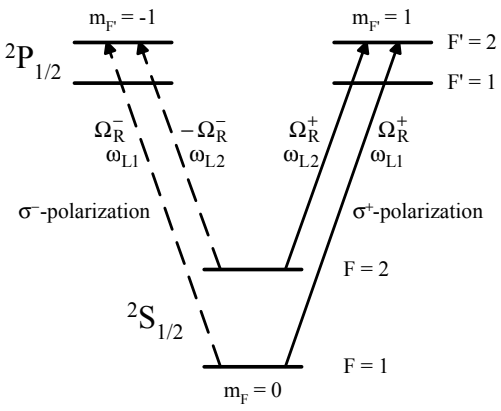

Fig. 1 Part of the energy levels of a ^{87}Rb atom associated with the D_1-line. The solid lines are frequency components with σ^+-polarization while the dashed lines represent frequency components with σ^--polarization. ω_{L1} and ω_{L2} are angular frequencies for the laser fields for CPT generation and detection. Ω_R^+ and Ω_R^- are Rabi frequencies for the transitions from the ground state to F' = 2, $m_{F'} = \pm 1$ states, respectively. See the text for discussion.

Without including the F' = 1 levels and the detuned transitions, the interaction Hamiltonian for this system is given by

$$\hat{H}_I \equiv \hat{H}_I{}^+ + \hat{H}_I{}^- \tag{4a}$$

where

$$\begin{aligned}\hat{H}_I{}^+ = &\frac{1}{2}\hbar\Omega_R^+ e^{-i\omega_{L1}t}|F'=2, m_{F'}=+1\rangle\langle F=1, m_F=0| \\ &+\frac{1}{2}\hbar\Omega_R^+ e^{-i\omega_{L2}t}|F'=2, m_{F'}=+1\rangle\langle F=2, m_F=0| \\ &+\text{h.c.}\end{aligned} \tag{4b}$$

$$\begin{aligned}\hat{H}_I{}^- = &\frac{1}{2}\hbar\Omega_R^- e^{-i\omega_{L1}t}|F'=2, m_{F'}=-1\rangle\langle F=1, m_F=0| \\ &-\frac{1}{2}\hbar\Omega_R^- e^{-i\omega_{L2}t}|F'=2, m_{F'}=-1\rangle\langle F=2, m_F=0| \\ &+\text{h.c.}\end{aligned} \tag{4c}$$

Notice that the second term in (4c) has a minus sign because the atomic symmetry gives

$$\begin{aligned}&\langle F=2, m_F=0|-e\vec{r}|F'=2, m_{F'}=-1\rangle = \\ &-\langle F=2, m_F=0|-e\vec{r}|F'=2, m_{F'}=+1\rangle\end{aligned} \tag{5}$$

In this case, the dark state described by (2) for σ^+ polarization light becomes

$$\begin{aligned}|\text{dark state}^+\rangle = &\frac{1}{\sqrt{2}}e^{i\omega_{L1}t}|F=1, m_F=0\rangle \\ &-\frac{1}{\sqrt{2}}e^{i\omega_{L2}t}|F=2, m_F=0\rangle\end{aligned} \tag{6}$$

which satisfies

$$\langle F'=2, m_{F'}=1|\hat{H}_I{}^+|\text{dark state}^+\rangle = 0 \tag{7}$$

However the same state is not a dark state with respect to the interaction Hamiltonian (4c). In fact, we have

$$\langle F'=2, m_{F'}=-1|\hat{H}_I{}^-|\text{dark state}^+\rangle = \frac{1}{\sqrt{2}}\hbar\Omega_R^- \tag{8}$$

i.e., the two terms in (4c) add together coherently to enhance each other due to the coherence described by (6). Therefore it is expected that the σ^--polarization light experiences more attenuation when the CPT resonance condition is satisfied.

For the state |F'=1>, we have

$$\left\langle F=1, m_F=0\left|-e\vec{r}\right|F'=1, m_{F'}=-1\right\rangle = -\left\langle F=1, m_F=0\left|-e\vec{r}\right|F'=1, m_{F'}=+1\right\rangle \quad (9)$$

Again the σ^--polarization light suffers more attenuation when the CPT resonance condition is satisfied.

Similarly, the optical phase shift for the σ^--polarization light due to CPT resonance has an opposite sign from the one for the σ^+-polarization light because of the Kramers-Kronig relations.

In the ^{87}Rb atom, there are 16 energy levels involved when the D_1-line is used for CPT-generation and CPT-detection. Numerical calculations are used to study such a system. The calculations include all the velocity distribution of the atomic vapor in an optically-thick absorption cell. The calculations assume that the laser intensity is uniform across the laser beam. The dephasing process for both optical transitions and microwave transitions are determined according to the buffer gas condition and the cell geometry. Figure 2(a) and 2(b) show the normalized laser beam intensities for the σ^+- polarization and σ^--polarization, respectively. Figure 3(a) and 3(b) show the accumulated phase for the laser fields with the σ^+-polarization and σ^--polarization, respectively.

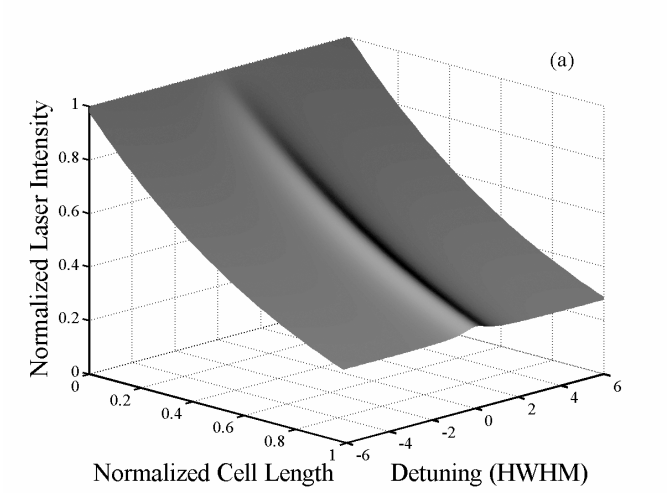

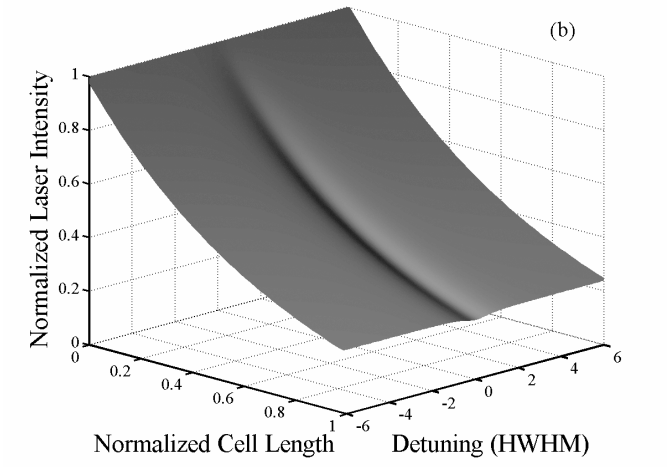

Fig. 2 Numerical calculation results for the laser frequency component with an angular frequency ω_{L1}: (a) Normalized intensity for the σ^+-polarization. (b) Normalized intensity for the σ^--polarization.

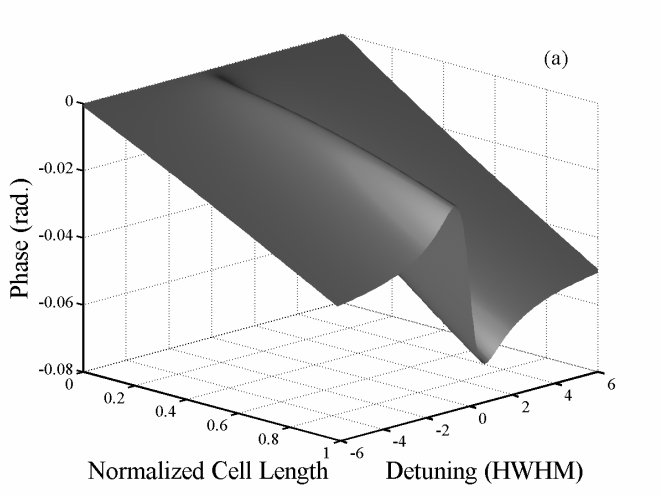

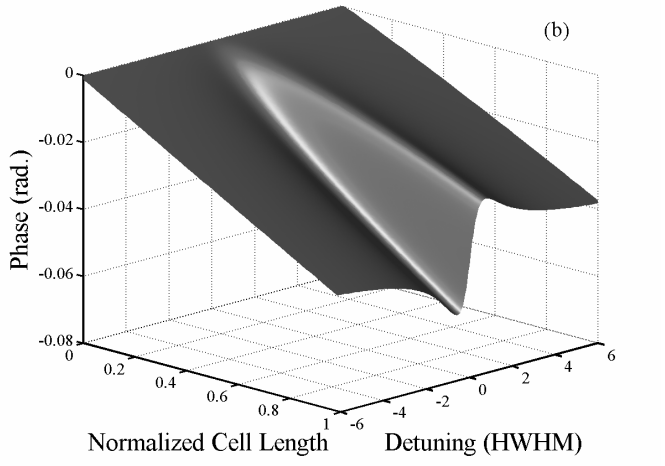

Fig. 3 Numerical calculation results for the laser frequency component with an angular frequency ω_{L1}: (a) Accumulated phase due to rubidium vapor in the cell for the σ^+-polarization. (b) Accumulated phase due to rubidium vapor in the cell for the σ^--polarization.

B. Polarization-Selective Detection Method [1]

To analyze the polarization state of the laser beam emerging from the absorption cell, we assume that the laser beam propagates along the quantization axis, which is defined by the external magnetic field. The electric field for one of the

CPT-generating frequency components can be written as

$$\vec{E} \approx \hat{e}^{+}E^{+}e^{-i\omega t-i\varphi^{+}}\ \exp\left\{i\frac{\omega}{c}l_c\sqrt{1+\chi^{+}(\delta)}\right\} + \hat{e}^{-}E^{-}e^{-i\omega t-i\varphi^{-}}\ \exp\left\{i\frac{\omega}{c}l_c\sqrt{1+\chi^{-}(\delta)}\right\} \tag{10}$$

where $\hat{e}^{+}$ ($\hat{e}^{-}$), E^{+} (E^{-}), and φ^{+} (φ^{-}) are the unit polarization vector, the amplitude of the electric field, and the phase for σ^{+}-polarization (σ^{-}-polarization), respectively, ω is the angular frequency of this frequency component, and l_c is the length of the absorption cell. In (10) the atomic susceptibilities

$$\chi^{\pm}(\delta) \equiv \chi^{\pm}{}'(\delta) + i\chi^{\pm}{}''(\delta) \tag{11}$$

are functions of both the optical frequency ω and the microwave detuning $\delta \equiv \omega_{L1} - \omega_{L2} - \omega_{HFS}$. However, in the vicinity of $\delta = 0$, the atomic susceptibilities do not vary with ω rapidly due to broader optical transition linewidth. Therefore we include the non-CPT related contribution of the atomic susceptibilities into $E^{\pm}$ and $\varphi^{\pm}$ in (10) and only show the CPT-related part explicitly in (10) and (11).

The CPT-related part of the atomic susceptibilities in (11) can be written in terms of on-resonance absorption coefficients $\alpha_0^{\pm}$ as

$$\chi^{\pm}(\delta) = \alpha_0^{\pm}\gamma_\mu\frac{c}{\omega}\left\{-\frac{\delta}{\delta^2+{\gamma_\mu}^2}+i\frac{\gamma_\mu}{\delta^2+{\gamma_\mu}^2}\right\} \tag{12}$$

where γ_μ is the linewidth (HWHM) of the CPT resonance signal.

After passing though a proper waveplate, the σ^{+}-polarization (σ^{-}-polarization) in (10) is converted into a linear polarization along the x-axis (y-axis). In addition, the waveplate introduces a relative phase shift, φ_w, between the two polarizations. The electric field of the frequency component exiting a polarization analyzer with its passing axis aligned parallel to the direction of $\hat{e}_\theta$ (Fig. 4) is

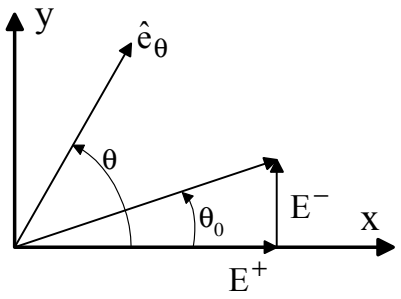

Fig. 4 Diagram showing the polarization states. See the text for discussion.

$$E_\theta \approx e^{-i\omega t-i\varphi^{+}}\left\{E^{+}\cos\theta\exp\left\{i\frac{\omega}{c}l_c\left[1+\frac{1}{2}\chi^{+}{}'+\frac{1}{2}i\chi^{+}{}''\right]\right\} + E^{-}\sin\theta\exp\left\{i\frac{\omega}{c}l_c\left[1+\frac{1}{2}\chi^{-}{}'+\frac{1}{2}i\chi^{-}{}''\right]+i\psi\right\}\right\} \tag{13}$$

where $\psi \equiv \varphi^{+} - \varphi^{-} + \varphi_w$. Choosing $\theta = \theta_0 + \zeta - \pi/2$ with $\theta_0 \equiv \tan^{-1}[E^{-}/E^{+}]$ we write (13) as

$$E_{\theta=\theta_0+\zeta-\pi/2} \approx e^{-i\omega t-i\varphi^{+}}\exp\left\{i\frac{\omega}{c}l_c\right\}\sqrt{{E^{+}}^2+{E^{-}}^2}\times\{\sin\zeta + i\left[\cos\theta_0\sin(\theta_0+\zeta)\,\xi^{+}{}'-\sin\theta_0\cos(\theta_0+\zeta)\left(\xi^{-}{}'+\psi\right)\right] - \cos\theta_0\sin(\theta_0+\zeta)\,\xi^{+}{}''+\sin\theta_0\cos(\theta_0+\zeta)\,\xi^{-}{}''\} \tag{14}$$

where $\xi^{\pm}{}' \equiv \frac{\omega}{2c}l_c\,\chi^{\pm}{}'$ and $\xi^{\pm}{}'' \equiv \frac{\omega}{2c}l_c\,\chi^{\pm}{}''$. It is seen from (14) that the CPT resonance signal in the photocurrent is somewhat skewed unless $\psi = 0$.

Since we are interested in blocking most of power in the AC Stark shift controlling frequency components, we prefer to align the passing axis of the polarization analyzer so that $\zeta \approx 0$. Particularly for $\zeta = 0$, the photocurrent is

$$I_\theta \propto \frac{1}{4}\left[{E^{+}}^2+{E^{-}}^2\right](\sin 2\theta_0)^2\times\left\{\left[\left(\chi^{-}{}''-\chi^{+}{}''\right)\frac{\omega}{2c}l_c\right]^2 + \psi^2+\psi\left(\chi^{-}{}'-\chi^{+}{}'\right)\frac{\omega}{c}l_c+\left[\left(\chi^{-}{}'-\chi^{+}{}'\right)\frac{\omega}{2c}l_c\right]^2\right\} \tag{15}$$

Using (12), we write (15) in the form of

$$I_\theta \propto \frac{1}{4}\left[{E^{+}}^2+{E^{-}}^2\right](\sin 2\theta_0)^2\times\left\{\psi\left(\alpha_0^{+}-\alpha_0^{-}\right)\frac{\delta\gamma_\mu}{\delta^2+{\gamma_\mu}^2}l_c + \psi^2+\frac{1}{4}\left(\alpha_0^{+}-\alpha_0^{-}\right)^2\frac{{\gamma_\mu}^2}{\delta^2+{\gamma_\mu}^2}{l_c}^2\right\} \tag{16}$$

III. Experiments

Figure 5 shows the block diagram of the experimental setup. A single frequency diode laser is frequency modulated by coupling a microwave signal into the injection current. The

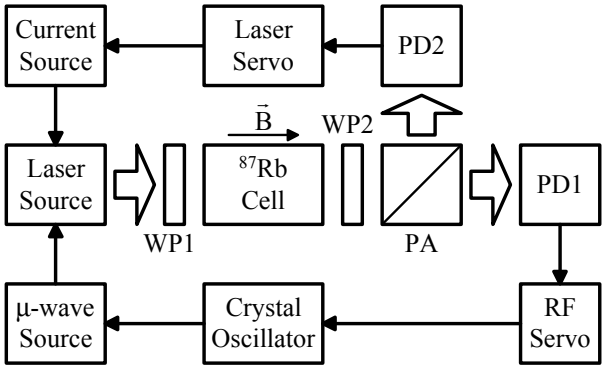

Fig. 5 Block diagram of the experiment setup: PA is a polarization analyzer. WP1 and WP2 are two waveplates. PD1 and PD2 are photo-detectors.

±1st order sidebands serve as the CPT-generation and CPT-detection frequencies while the higher order sidebands suppress the AC Stark shift [4]. The first waveplate (WP1) converts the linear polarization of the laser output beam to the desired elliptical polarization so that most of the power is in the σ^+-polarization for CPT generation. The second waveplate (WP2), which is a combination of three linear waveplates, converts the circular polarizations of the laser fields emerging from the absorption cell into the desired linear polarizations, and provides the necessary relative phase shift between the two orthogonal polarizations. The waveplate WP2 and the polarization analyzer (PA) are aligned so that the polarization analyzer blocks most of the power in AC Stark shift suppression frequency components and the CPT resonance signal is symmetric.

For the first part of the experiment, the microwave frequency is scanned across the CPT resonance frequency. The output of the photo-detector (PD1) is recorded. Figure 6 shows a typical data set. A contrast of 22% and a linewidth

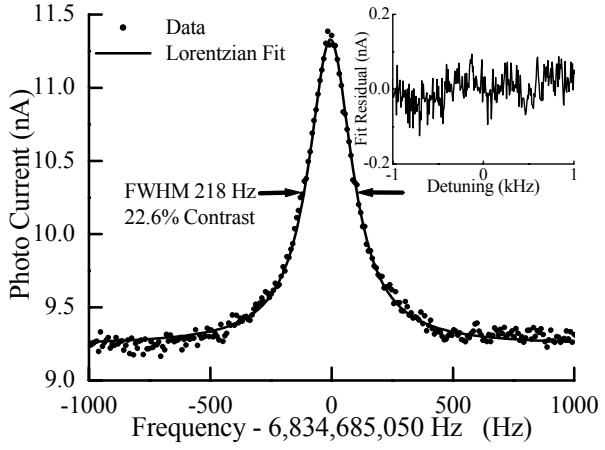

Fig. 6 CPT resonance signal detected using the polarization-selective method. A Lorentzian line-shape is fit to the experimental data. The fitting residual is also shown.

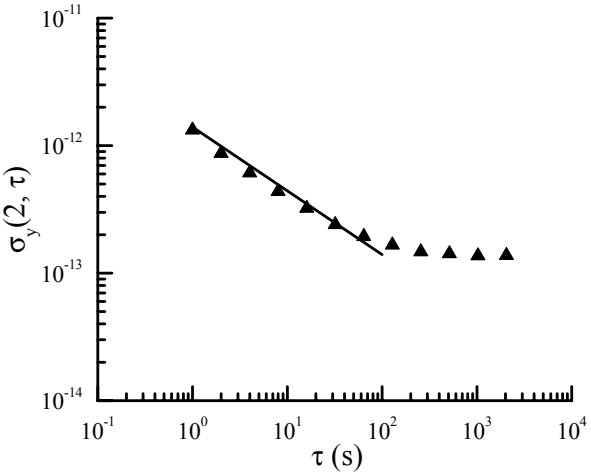

Fig. 7 Allan deviation of the CPT-based rubidium frequency standard using the polarization-selective detection method. ▲ is the measured Allan deviation using a diode laser pumped rubidium frequency standard as a reference. The solid line is $1.4 \times 10^{-12}\ \tau^{-1/2}$.

of 218 Hz (FWHM centered at the ^{87}Rb hyperfine transition frequency 6.8 GHz) are achieved.

In the second part of the experiment, the resonance frequency of the CPT signal, which is derived by using the polarization-selective detection method, serves as the reference frequency for locking the frequency of the crystal oscillator. Figure 7 shows the Allan deviation of this CPT-based rubidium frequency standard with the polarization-selective detection method. When using a laser pumped rubidium frequency standard as a reference, Fig. 7 shows the measured short term stability is $1.4 \times 10^{-12}\ \tau^{-1/2}$. The measurement of the signal-to-noise ratio in the reference rubidium frequency standard shows that the reference standard has a similar short term stability as the one of the CPT-based rubidium frequency standard. Therefore it is expected that the CPT-based rubidium frequency standard has a somewhat better short term stability than the directly measured result of $1.4 \times 10^{-12}\ \tau^{-1/2}$.

IV. Conclusion

A high contrast CPT resonance signal is obtained using a polarization-selective method. In this method a single laser beam is used for CPT generation and detection while keeping the AC Stark shift suppressed. The detection method is used in a vapor cell rubidium frequency standard to demonstrate a measured Allan deviation of $1.4 \times 10^{-12}\ \tau^{-1/2}$.

Acknowledgment

The author thanks Len Cutler and Robin Giffard for their support of the project and for many stimulating and fruitful discussions. The author thanks John (Jack) Kusters for his interest in this project and for his supply of some optics used in the experiments. The author is grateful to Jim Johnson and

Ray Wong for their help with building some electronics for this project.

REFERENCES

[1] U. S. Patent pending.
[2] N. Cyr, M. Têtu, and M. Breton, IEEE Tran. Instrum. Meas. **42**, 640 (1993).
[3] J. Vanier, A. Godone, and F. Levi, Phys. Rev. **A58**, 2345 (1998).
[4] M. Zhu and L. S. Cutler, Proceedings of Precision Time and Time Interval 2000, Reston, Virginia, p. 311.
[5] M. Zhu and L. S. Cutler, US Patent 6,201,821.
[6] M. Zhu and L. S. Cutler, US Patent 6,363,091.
[7] G. Orriols, Nuovo Cimento, **B53**, 1 (1979).
[8] E. Arimondo, in *Progress in Optics*, edited by E. Wolf (Elsevier, Amsterdam, 1996), Vol. 35, p. 257.
[9] E. U. Condon and G. H. Shortley, *The Theory of Atomic Spectra*, Cambridge University Press, 1935.
[10] A. R. Edmonds, *Angular Momentum in Quantum Mechanics*, Princeton University Press, 1974.
[11] W. Happer, Rev. Mod. Phys. **44**, 169 (1972).
[12] C. Wieman and T. W. Hänsch, Phys. Rev. Lett. **36**, 1170 (1976).